PLOS ONE

RESEARCH ARTICLE

The polymorphism of *Hydra* microsatellite sequences provides strain-specific signatures

Quentin Schenkelaars¤, Diego Perez-Cortes, Chrystelle Perruchoud, Brigitte Galliot*

Department of Genetics and Evolution, Institute of Genetics and Genomics in Geneva (iGE3), University of Geneva, Geneva, Switzerland

¤ Current address: Jacques Monod Institute, Paris, France
* brigitte.galliot@unige.ch

Citation: Schenkelaars Q, Perez-Cortes D, Perruchoud C, Galliot B (2020) The polymorphism of *Hydra* microsatellite sequences provides strain-specific signatures. PLoS ONE 15(9): e0230547. https://doi.org/10.1371/journal.pone.0230547

Editor: Robert E. Steele, University of California Irvine, UNITED STATES

Received: March 1, 2020

Accepted: September 4, 2020

Published: September 28, 2020

Data Availability Statement: Sequences MN988633 to MN988642 corresponding to the 16S gene listed in S1 Table, sequences MT024252 to MT024260 corresponding to the COI gene listed in S1 Table, and sequences MT024261 to MT024300 listed in S2 Table are accessible at the URL: www.ncbi.nlm.nih.gov/genbank/.

Funding: SNF grants to Brigitte Galliot 31003A_169930; 310030_189122 Swiss National Fonds (SNF) http://www.snf.ch/en/Pages/default.aspx The funders had no role in study design, data

Abstract

Hydra are freshwater polyps widely studied for their amazing regenerative capacity, adult stem cell populations, low senescence and value as ecotoxicological marker. Many wild-type strains of *H. vulgaris* have been collected worldwide and maintained effectively under laboratory conditions by asexual reproduction, while stable transgenic lines have been continuously produced since 2006. Efforts are now needed to ensure the genetic characterization of all these strains, which despite similar morphologies, show significant variability in their response to gene expression silencing procedures, pharmacological treatments or environmental conditions. Here, we established a rapid and reliable procedure at the single polyp level to produce via PCR amplification of three distinct microsatellite sequences molecular signatures that distinguish between *Hydra* strains and species. The TG-rich region of an uncharacterized gene (*ms-c25145*) helps to distinguish between Eurasian *H. vulgaris-Pallas* strains (*Hm-105*, *Basel1*, *Basel2* and *reg-16*), between Eurasian and North American *H. vulgaris* strains (*H. carnea*, *AEP*), and between the *H. vulgaris* and *H. oligactis* species. The AT-rich microsatellite sequences located in the *AIP* gene (*Aryl Hydrocarbon Receptor Interaction Protein*, *ms-AIP*) also differ between Eurasian and North American *H. vulgaris* strains. Finally, the AT-rich microsatellite located in the *Myb-Like cyclin D-binding transcription factor1* gene (*ms-DMTF1*) gene helps to distinguish certain transgenic *AEP* lines. This study shows that the analysis of microsatellite sequences, which is capable of tracing genomic variations between closely related lineages of *Hydra*, provides a sensitive and robust tool for characterizing the *Hydra* strains.

Introduction

Since the initial discovery of *Hydra* regeneration by Abraham Trembley in 1744 [1], the freshwater *Hydra* polyp is used as a fruitful model system not only in cell and developmental biology but also for aging, neurobiology, immunology, evolutionary biology and ecotoxicology studies [2–8]. *Hydra*, which belongs to Cnidaria, the sister phylum of bilaterians (**Fig 1A**), is closely related to jellyfish although displaying a life cycle restricted to the polyp stage (**Fig 1B**).

collection and analysis, decision to publish, or preparation of the manuscript.

Competing interests: The authors have declared that no competing interests exist.

Over the past 100 years, numerous strains were captured all over the world to explore the variability of the *Hydra* genus and the genetic basis of developmental mechanisms [9–11].

The analysis of morphological and cellular criteria identified in *Hydra* strains collected worldwide established four distinct groups named *H. oligactis* (stalked *Hydra*), *H. vulgaris* (common *Hydra*), *H. viridissima* (symbiotic green *Hydra*) and *H. braueri* (gracile *Hydra*) [11] (**Fig 1B**). The main cellular criterion was provided by the morphology of nematocysts (the venom capsules located inside the mature stinging cells named nematocytes or cnidocytes) that varies between the *Hydra* groups [12]. More recently, a series of mitochondrial and nuclear molecular markers were used for a series of phylogenetic analyses [13–16], which confirmed the relevance of these four groups but also revealed that each group may actually contain several closely related strains that have been described as different species, *e.g. H. carnea and H. vulgaris* within the *H. vulgaris* group (**Fig 1A**). Indeed, in this group, two sub-groups were identified, the *H. vulgaris-Pallas* sub-group that includes animals collected in Europe and Asia, typically the *Hv*_Basel and *H. magnipapillata 105 (Hm-105)* strains respectively, while the second sub-group named *H. vulgaris-4* by Schwentner and Bosch [16] includes animals

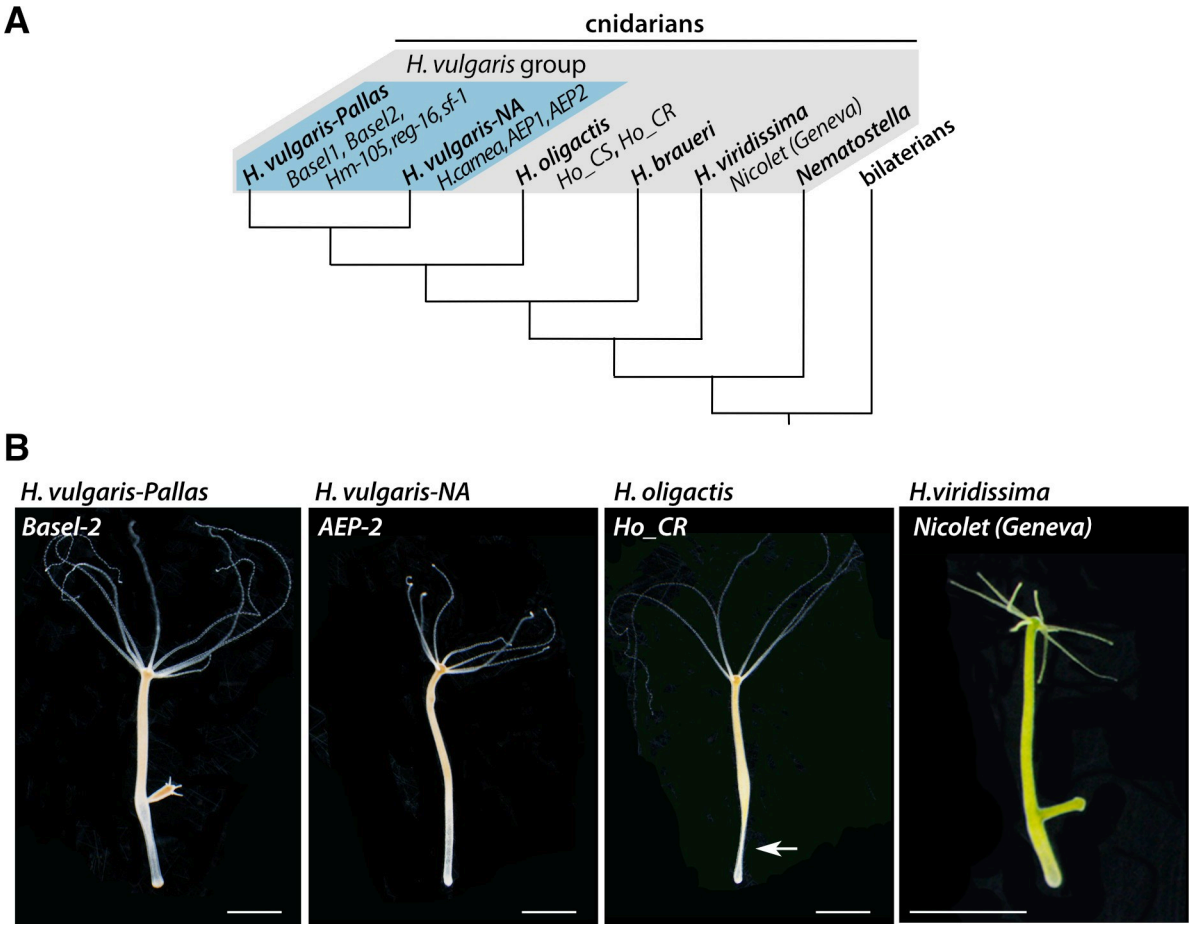

Fig 1. Phylogenetic position and morphology of the freshwater *Hydra* polyps. (A) Schematic view of the phylogeny of the four groups of *Hydra* species as reported in references 13–16: *H. vulgaris* with the sub-groups *H. vulgaris-Pallas* and *H. vulgaris-NA* (blue background), *H. oligactis*, *H. braueri*, and *H. viridissima*. **(B)** Images of polyps illustrating the similar overall appearance between strains and species despite differences in developmental and cellular responses: *H. vulgaris-Pallas (Basel-2 strain)*, *H. vulgaris-NA (AEP-2 strain)*, *H. oligactis (Cold-resistant strain, Ho_CR)* and *H. viridissima (Nicolet-Geneva strain)* groups. Note the stalk peduncle (arrow) typical of the *H. oligactis* species. Scale bars: 2 mm.

https://doi.org/10.1371/journal.pone.0230547.g001

collected in North America as *H. carnea* from which the AEP strain was derived (**Fig 1A**). In the absence of consensus names for the latter, we have decided to name it "*H.vulgaris-NA*", following their North American (NA) origin.

Among the *H. vulgaris-Pallas* species, the *H. magnipapillata* strain 105 (*Hm-105*) is a Japanese strain described by Ito in 1947 [17] and widely used since then [9, 14]. Several European *H. vulgaris* strains (*Basel*, *Zürich*, etc.) were also characterized [12], actually found closely related to the Asian *Hm-105* strain. The *AEP* strain, which constitutively produces gametes, was obtained by crossing two North American strains, most likely the *H. carnea* and *H. littoralis* strains [18], subsequently selected for transgenesis [19]. Nowadays, the laboratories that use *Hydra* as an experimental model maintain clonal cultures from *H. vulgaris-Pallas* (*Hm-105*, *sf-1*, *reg-16*, *Basel*, *Zürich*, *AEP* strains), *H vulgaris-NA* but also from *H. viridissima* (e.g. *Nicolet* as Geneva strain) or *H. oligactis* species (e.g. *Ho_CS*, *Ho_CR* as European strains) (**Fig 1B**). A facility located in Mishima (Japan) maintains for the scientific community specimens from a large variety of strains and species (molevo.sakura.ne.jp/Hydra/magni.html).

The importance of identifying the various *Hydra* strains/species relies on the fact that they can exhibit (i) different developmental behaviors, especially the morphogenetic variants that show distinct budding rate or size features in homeostatic context [20–23], (ii) lower regeneration potential such as the *reg-16* strain that was obtained through inbreeding of the Japanese *H. magnipapillata* strain [24], (iii) abnormal apical patterning such as multiheaded strains [25, 26], (iv) specific cellular properties such as the *nf-1* strain that contains neither interstitial stem cells nor interstitial derivatives [27] or the *sf-1* thermo-sensitive strain that loses its cycling interstitial cells upon transient heat-shock exposure [28]. Importantly, strains that do not show obvious differences at the morphological or cellular levels actually exhibit variable responses to gene silencing upon RNA interference [29], to drug treatment [30–32] or to environmental stresses [32]. In addition, experimental evidence indicate that strain-specific signals regulate the proliferation of interstitial cells [33].

During the past ten years, efforts were made to obtain the *H. vulgaris* genome [34], reference transcriptomes and proteomes [35–37], quantitative RNA-seq in homeostatic and regenerative conditions [38–41], on flow-cytometry sorted stem cell populations [38, 40–42] and single-cell transcriptomes [43]. Two strains of *H. oligactis*, one named "cold-sensitive" (*Ho_CS*) that undergoes aging and another named "cold-resistant" (*Ho_CR*) that does not, were used for transcriptomic and proteomic analysis [32]. Genomic sequences were also made available for the *H. oligactis* and *H. viridissima* species [41]. The current molecular barcoding in *Hydra* is precise and efficient but time-consuming and relatively costly as based on DNA extractions, PCRs amplification followed by DNA sequencing, and therefore not well-adapted to large-scale characterization of individual polyps.

Microsatellites consist in tandem repeats of short nucleotide motifs of variable length, e.g. (TA)n, (CA/TG)n, (CG)n, (CAG)n, where n represent the number of repetitions [44]. These microsatellites are distributed at different locations in the genome, and the number of repeats within a given microsatellite may differ between animals of the same species or population. As a result, microsatellites are widely used for DNA profiling in population genetics studies, but also in criminal investigations, paternity testing, or identification of individuals in the event of a mass disaster [45, 46]. In these studies, individuals with the same number of repeats at a given genomic location are considered to be closely related, while each additional repeat reflects a divergent step. The combined analysis of different microsatellites makes it possible to construct a genotypic fingerprint specific to each individual, which provides accurate information for tracing evolutionary events such as population bottleneck, migrations, expansions, etc. . .

The objective of this work was to establish a rapid, inexpensive and reliable method to characterize animals of the *H. vulgaris* strains used in the laboratory. To this end, we established a

Table 1. Sequences of the primers used in this study.

Gene name	Foward primer	Reverse Primer
16S	TCGACTGTTTACCAAAAACATAGC	ACGGAATGAACTCAAATCATGTAA
β-actin	GCTCTTCCCCATGCCATTAT	AGCTTGAAGCAGCAGTTTGC
COI	AAGTGTATAATTGAATCACACGTTG	CTTCAGGGTGACCAAAAAATCA
ms-c25145	GGAAGAGACAGATTCCCAAT	AATGCTCTTTCCTCACAGTC
ms-AIP	CGAGACAGCGTTTTCAAG	CCACTCTTCCATTCTAACCA
ms-DMTF1	ATCGATTTAACTGCTGAAGG	AACCAAATCACAGATTTAAAATAA

https://doi.org/10.1371/journal.pone.0230547.t001

method that relies on PCR amplification of microsatellite sequences on a single polyp without DNA extraction or sequencing. We show that the analysis of microsatellite polymorphism in animals from either various wild-type strains or transgenic lines provides specific signatures that reliably distinguish strains of the *H. vulgaris* group. This barcoding method, now routinely applied in our laboratory, is efficient and well suited for large-scale studies.

Materials and methods

Hydra strain collection

The wild-type strains used in this study were a kind gift from colleagues, *Basel1* and *AEP1* from B. Hobmayer (University of Innsbruck), *Basel2*, *Hm-105* and *Ho_CR* from T. Holstein (University of Heidelberg), *AEP2* from R. Steele (University of California), *Ho_CS* from H. Shimizu (National Institute of Genetics, Mishima) and *Nicolet* from a Geneva pond. The AEP transgenic lines that constitutively express GFP in their epithelial cells, either gastrodermal (*endo-GFP*) or epidermal (*ecto-GFP*), were produced by the Bosch Lab (University of Kiel) [19, 47] and kindly provided to us. The *AEP1* transgenic lines expressing the *HyWnt3–2149*::*GFP* construct (here named *Wnt3*::*GFP*) either in epidermal or gastrodermal epithelial cells were produced in-house with the *HyWnt3–2149*::*GFP-HyAct*:*dsRed* reporter construct kindly given by T. Holstein [48, 49]. We also produced in the AEP2 strain the Q82-203 and Q82-293 lines by injecting early embryos with the *HyActin*:*Q82-eGFP* construct (QS, unpublished) following the original procedure [19]. All cultures were fed three times a week with freshly hatched *Artemia* and washed with *Hydra* Medium (HM) [24].

One-step preparation of macerate extracts

Live polyps were washed three times five minutes in distilled water. Then, single polyps were dissociated into 50 μL distilled water by energetically pipetting them up and down until there is no tissue left, and immediately transferred on ice. Alternatively, reg-16 polyps previously fixed in paraformaldehyde (PFA 4%) and stored in methanol for several months, were stepwise rehydrated and dissociated as indicated above. Cell density of each macerate was estimated by measuring the OD_{600} using a NanoDrop One (Thermo Sientific). The DNA content and DNA purity were roughly estimated by measuring the absorbance of each sample at 230, 260 and 280 nm. To implement an efficient one-step PCR procedure, we selected three *AEP2* polyps showing a regular size (about 4–6 mm long without the tentacles).

PCR amplification from macerate extracts

To test the efficiency of PCR amplification on macerate extracts, we used primers of the *β-actin* gene (**Table 1**) on 0, 0.5, 1.5, 5 and 15 μL macerate extract as template for a final 25 μL PCR mix (1x Taq Buffer, 1x Coral Load, 400 nM of each primer, 160 nM dNTPs and 0.5 unit

of Top Taq Polymerase, Qiagen). Subsequently we used 5 μL out of 50 μL macerate extract to amplify the mitochondrial *cytochrome C oxidase I* (*COI*) gene, the mitochondrial *16S ribosomal DNA* (*16S*) and the microsatellite regions (ms) in each strain (**Table 1**, **S1 Table**). Similar PCR conditions were used for all amplifications. Briefly, after an initial denaturation step at 94˚C for two minutes, samples were submitted to 30 cycles of (i) denaturation at 94˚C for 15 seconds, (ii) annealing at 52˚C for 30 seconds and (iii) a 30–60 seconds elongation step at 72˚C. The process was terminated by a final extension at 72˚C for 15 minutes. 10 μL PCR products were run on a 2.5% agarose gel at 120 V for two to three hours in the case of microsatellites, stained with ethidium bromide and revealed under UV-light.

Cloning and sequencing

For sequence validation, the PCR products were cloned using the pGEMT kit (Promega): 3 μl PCR products were ligated to 50 ng pGEMT vector in the presence of 3 units T4 ligase overnight at 18˚C (final volume 10 μL). Plasmidic DNA was integrated into competent DH5α *E. coli* and colonies were screened thanks to alpha-complementation. After overnight culture, plasmidic DNA was extracted using the CTAB procedure and sequenced using standard T7 primer at Microsynth (Basel, Switzerland). The number of colonies we sequenced and their origin (single or several animals) is indicated for each microsatellite sequence in **S2 Table**.

Phylogenetic analyses

The *COI* and *16S* genes were selected for phylogenetic analyses. Corresponding DNA sequences were amplified by direct PCR amplification method as described above and sequenced (**S1 Table**). The obtained sequenced were aligned with the dataset previously produced by Martinez et al. [15] using the ClustalW function of BioEdit v7.2.6.1, and Maximum Likelihood phylogenetic trees were constructed with the PhyML 3.0 software (http://www.atgc-montpellier.fr/phyml/) applying the GTR substitution model [50]. The robustness of the nodes was tested by 1000 bootstraps.

Results

One-step genomic amplification after quick mechanical tissue maceration

To bypass genomic and mitochondrial DNA extractions that are time-consuming and expensive when massively performed, we established a rapid animal dissociation in water that provides genomic DNA of sufficient quantity and quality for PCR reaction. We obtained an efficient PCR amplification of *β-actin* (193 bp) from macerate extracts, indicating that the application of a mechanical force to dissociate the tissues combined to the initial denaturation step of the PCR reaction suffice to release high quality genomic DNA and amplify sequences of interest (**Fig 2A**). Despite slight variations in band intensity, certainly reflecting the amount of starting material, the amplification remained highly efficient whatever the polyp size, the 260/280 and 260/230 OD value ratios and the template volume used here (yellow dots **Fig 2B**). For all subsequent experiments, we used one tenth of macerate extract as template for *COI*, *16S* and microsatellite amplifications (**Fig 2B**). We also obtained efficient PCR amplification from macerate extracts prepared from animals fixed months or years earlier in paraformaldhehyde (PFA) and stored in methanol at -20˚C, especially for mitochondrial DNA amplification. This procedure thus allows us to gain genetic information from fresh as well as old samples.

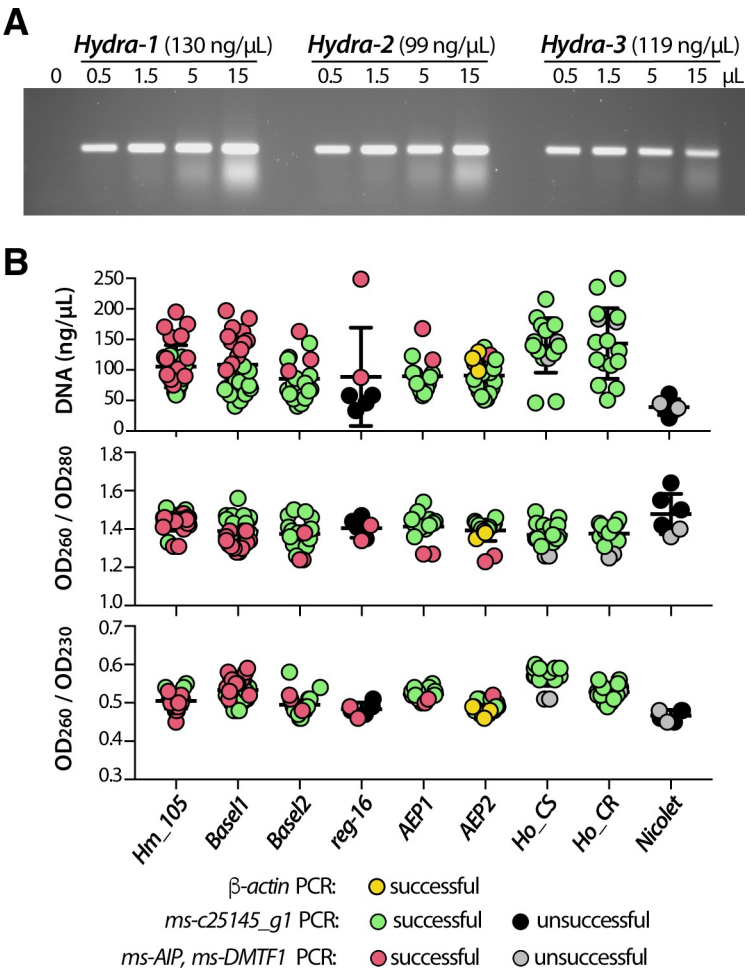

Fig 2. Direct genomic DNA amplification from single *Hydra* polyp. (A) PCR amplification of *β-actin* genomic DNA from three 4–6 mm long, non-budding AEP animals dissociated and resuspended each in 50 µl water. Various amounts (from 0 to 15µL) of the resulting macerates were used as PCR template for β-actin amplification to estimate PCR efficiency. **(B)** Graphic representation of DNA concentration and DNA purity as deduced from OD measurements at 260, 230 and 280 nm wave lengths. Each dot represents either the OD260 value or the 260/280 or 260/230 OD value ratios obtained from a single polyp. For each DNA, the efficiency of PCR amplification is indicated with a color code. Note the lower DNA content in most *reg-16* polyps that were fixed in PFA and stored in methanol for months prior to rehydration, maceration and DNA amplification.

https://doi.org/10.1371/journal.pone.0230547.g002

Phylogenetic assignation of *Hydra* strains to the different groups and species

Next, we confirmed the assignation of each strain we acquired to one of the four *Hydra* groups previously described (i.e. *H. vulgaris*, *H. oligactis*, *H. viridissima*, *H. braueri*), and when relevant to the species identified within each group, namely *H. vulgaris*-Pallas and *H. vulgaris-NA* within the *H. vulgaris* group [13–16]. Briefly, we performed phylogenetic analyses of the *COI* and *16S* sequences, efficiently amplified from one single polyp per strain of interest (*AEP1*, *AEP2*, *Basel1*, *Basel2*, *Hm-105*, *reg-16*, *Ho-CR*, *Ho-CS*, *Nicolet*) as detailed above. The global topology of the *COI* tree retrieves the four orthologous groups (**Fig 3**), which is not the case in the *16S* analysis where the *H. vulgaris* group actually includes the *H. brauerei* and *H. oligactis* groups that thus do not appear monophyletic (**S1 Fig**).

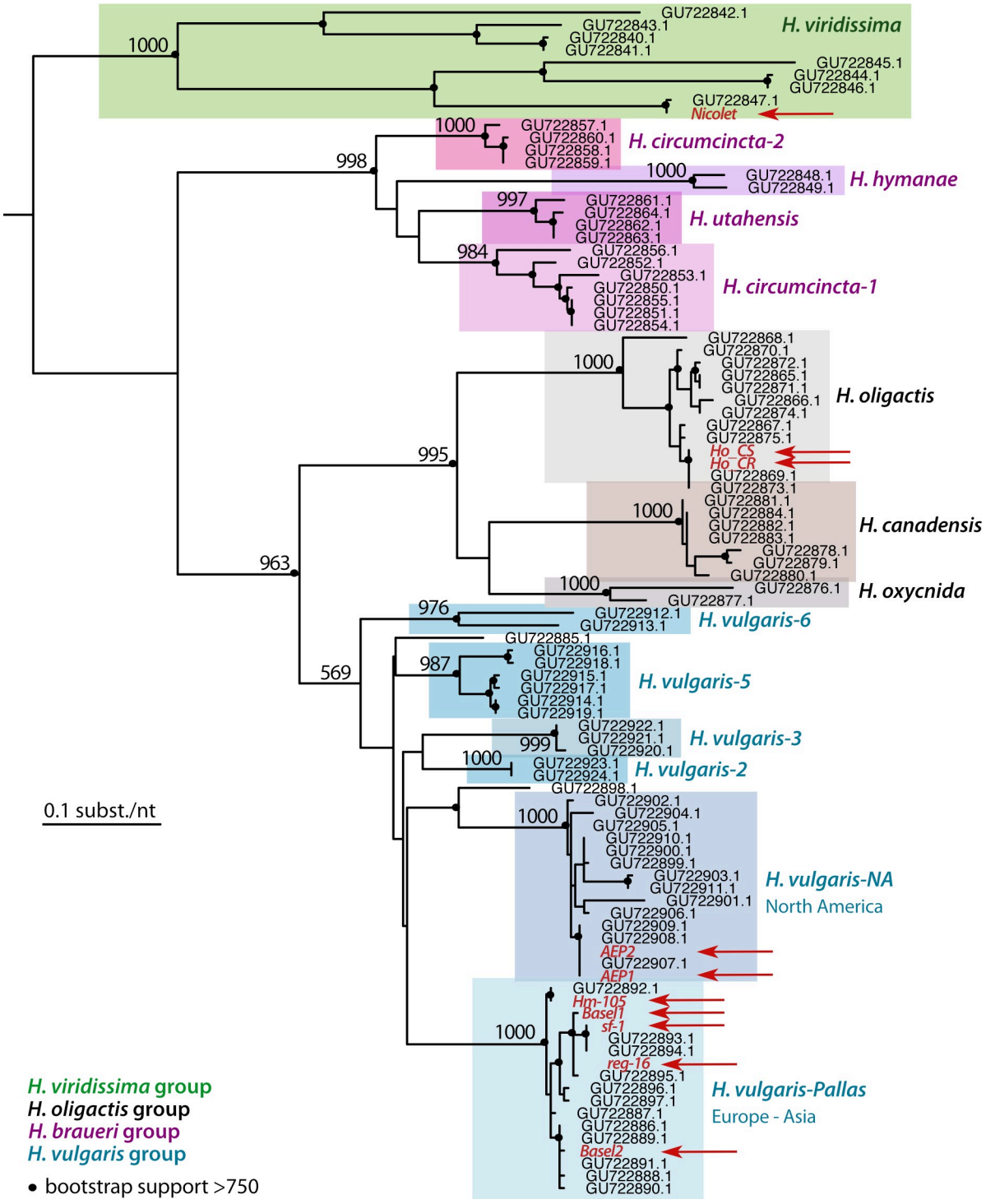

Fig 3. Phylogenetic relationships within the *Hydra* genus based on the analysis of the *Cytochrome Oxydase I (COI)* DNA sequences. The maximum likelihood tree of the *COI* sequences was built by adding to the dataset of 85 COI sequences available on Genbank [15] the 10 sequences obtained in the present study (written red, indicated with red arrows, see S2 Table for accession numbers). Black dots indicate the robustness of the nodes as deduced from the bootstrap support (at least 750 over 1'000 bootstraps). This tree confirms that the sequences obtained in this study distribute into the expected *Hydra* groups, *Nicolet* strain in *H. viridissima*, *Ho_CR* and *Ho_CS* in *H. oligactis*, *Hm-105*, *sf-1*, *reg-16*, *Basel-1* and *Basel-2* in *H. vulgaris-Pallas*, *AEP1*, *AEP2* in the *H.vulgaris-NA* sub-group.

https://doi.org/10.1371/journal.pone.0230547.g003

However, in both analyses, the sequences of the strains tested were grouped as expected within the 13 species previously identified (i.e. *H. circumcincta 1 and 2*, *H. hymanae*, *H. utahensis*, *H. oligactis*, *H. canadensis*, *H. oxycnida*, *H. vulgaris-1* to *H. vulgaris*-6). As expected, the *Hm-105* and *Hv_Basel* sequences belong to the *H. vulgaris-Pallas* sub-group that contains the *Hm-105* reference sequences (GU722892.1 for COI and GU722807.1 for 16S), whereas the *Ho_CS* and *Ho_CR* sequences both belong to the *H. oligactis* group, and the *Nicolet* sequences to the *H. viridissima* group. This analysis also confirms that the *AEP* sequences (*AEP1*, *AEP2*) belong to the *H. vulgaris-NA* sub-group (Fig 3). We found that the genomic *16S* sequences of the two *Hv_Basel* strains are identical, while the mitochondrial *COI* sequences are different with 9 mismatches out of 657 bp (sequences obtained twice independently). Consequently, animals of these two cultures can be considered as representatives of two different strains, which we have named *Basel1* and *Basel2*. In contrast, the *COI* and *16S* sequences of *AEP1* and *AEP2* are identical, suggesting that they could represent a single strain.

Identification of three microsatellite regions in the *Hydra vulgaris* genome

We then analyzed some microsatellite sequences to test the conclusions obtained in the phylogenetic analyses and to establish a method for easy identification of strains belonging to the *H. vulgaris* group. To identify *H. vulgaris* genomic regions that contain microsatellites, we blasted two different tandem repeat motifs $(TA)_{15}$ and $(CA)_{15}$ against *AEP* transcriptomes available at the HydrATLAS web portal. We found three transcripts expressed by *AEP* polyps that encode repeats, the first one *c25145_g1_i04* contains TG-repeats in its first intron (Fig 4, S2 Fig), the second *c8134_g1_i1* encodes the Aryl-hydrocarbon receptor-Interacting Protein (AIP) and contains AT-repeats in its 5' untranslated region (UTR) (Fig 5, S5 Fig), and the third one (*c21737_g1_i4*) encodes the cyclin-D-binding Myb-like Transcription Factor 1 (DMTF1) and contains AT-repeats located in the 3'UTR (Fig 6, S6 Fig).

Next, we validated these sequences onto genomic and transcriptomic databases publicly available for *Hm-105* on National Human Genome Research Institute (NHGRI) and Compagen. These three microsatellite regions were selected as they were retrieved from most databases and contained a variable number of microsatellite repeats between *H. vulgaris-Pallas (Hm-105)* and *H. vulgaris-NA (AEP)*. We named these microsatellite regions *ms-c25145*, *ms-AIP* and *ms-DMTF1* respectively; access to the corresponding transcriptomic and genomic sequences are given in S2 Table.

The *ms-c25145* polymorphism helps to discriminate between *Hydra* species and *H. vulgaris* strains

The TG-rich *ms-c25145* could be detected within two different *Hm-105* genomic regions (*Sc4wPfr_1246*, *Sc4wPfr_396* scaffolds) and the direct PCR approach efficiently amplified the *ms-c25145* genomic sequences in seven strains (*Hm-105*, *Basel1*, *Basel2*, *AEP1*, *AEP2*, *Ho_CS*, *Ho_CR*), but remained inefficient in the *reg-16* strain (*H. vulgaris* group), possibly as a consequence of a lower quality of the genomic DNA that was produced from animals stored in methanol after PFA fixation. Even though the primers were designed for the *H. vulgaris* group, we succeeded to amplify this region in samples from *Ho_CS* and *Ho_CR (H. oligactis* group), whereas no amplification was observed from gDNA freshly prepared from *Nicolet* animals (*H. viridissima* group), possibly due to mismatches into primer regions (Fig 4A, S3 Fig).

The patterns obtained for *ms-c25145* are quite different between *Hm-105* (four bands), *Basel1* (three bands) and *Basel2* (single band), indicating that these strains can indeed be considered as distinct, in agreement with the results of the *COI* phylogeny (Fig 3). Concerning the *AEP1* and *AEP2* strains, the *ms-c25145* patterns appear quite similar, with a main band about

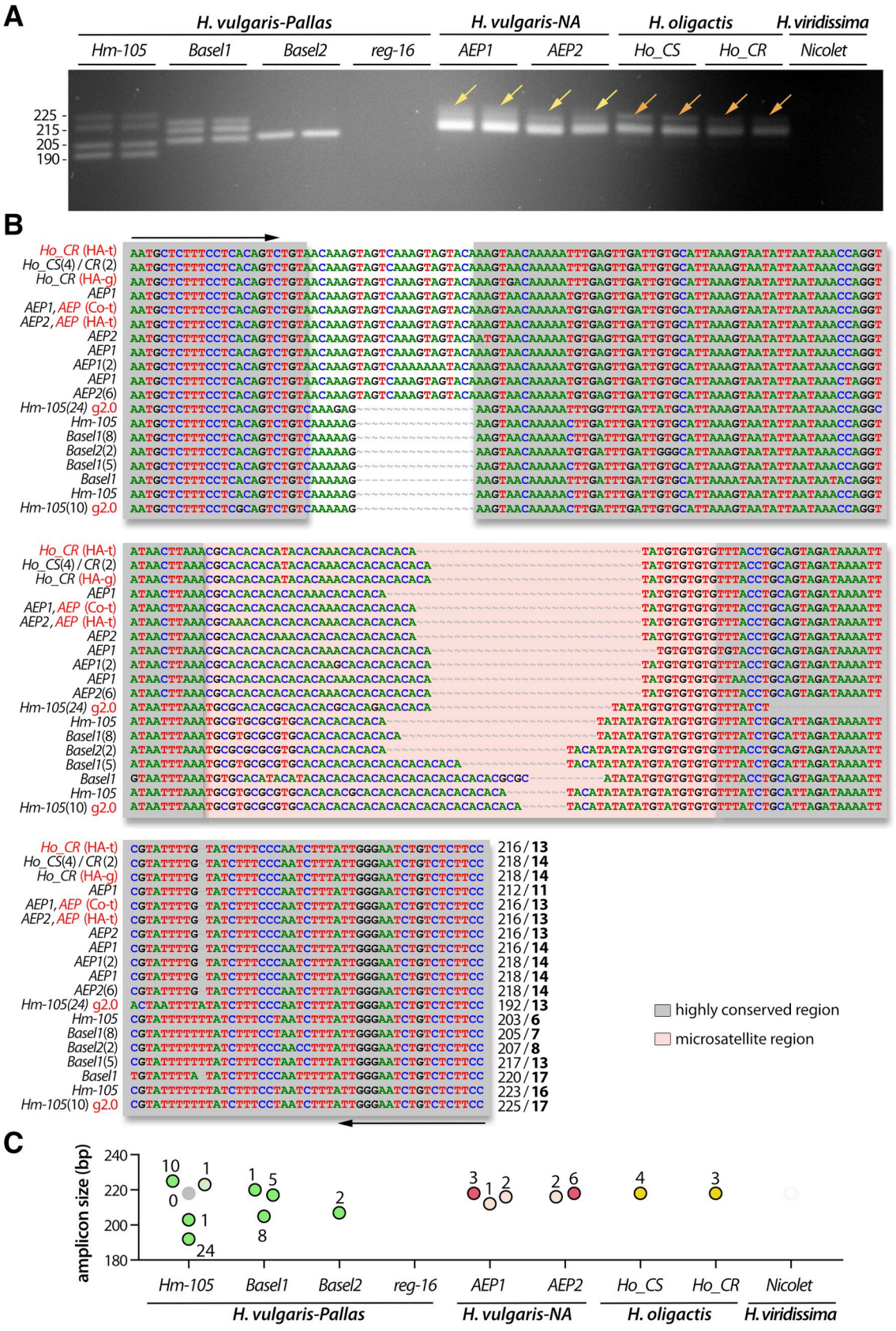
A
H. vulgaris-Pallas
H. vulgaris-NA
H. oligactis
H. viridissima
Hm-105
Basel1
Basel2
reg-16
AEP1
AEP2
Ho_CS
Ho_CR
Nicolet
225 -
215 -
205 -
190 -
B
Ho_CR (HA-t)
Ho_CS(4) / CR(2)
Ho_CR (HA-g)
AEP1
AEP1, AEP (Co-t)
AEP2, AEP (HA-t)
AEP2
AEP1
AEP1(2)
AEP1
AEP2(6)
Hm-105(24) g2.0
Hm-105
Basel1(8)
Basel2(2)
Basel1(5)
Basel1
Hm-105
Hm-105(10) g2.0
216 / 13
218 / 14
218 / 14
212 / 11
216 / 13
216 / 13
216 / 13
216 / 14
218 / 14
218 / 14
218 / 14
192 / 13
203 / 6
205 / 7
207 / 8
217 / 13
220 / 17
223 / 16
225 / 17
highly conserved region
microsatellite region
C
amplicon size (bp)
240
220
200
180
10
1
0
1
24
1
5
8
2
3
1
2
2
6
4
3
Hm-105
Basel1
Basel2
reg-16
AEP1
AEP2
Ho_CS
Ho_CR
Nicolet
H. vulgaris-Pallas
H. vulgaris-NA
H. oligactis
H. viridissima

Fig 4. Analysis of the polymorphism of the TG-rich microsatellite *c25145* sequence (*ms-c25145*). (A) Amplification of the *ms-c25145* genomic sequences from 7/9 tested strains that represent *H. vulgaris-Pallas* (*Hm-105*, *Basel1*, *Basel2* strains), *H. vulgaris-NA* (*AEP1*, *AEP2* strains) and *H. oligactis* (*Ho_CR*, *Ho_CS* strains). Yellow arrows point to a smear detected in both *AEP1* and *AEP2*, orange arrows point to a faint second band detected in both *Ho_CS* and *Ho_CR*. **(B)** Sequence alignment of the *ms-c25145* region. The salmon-pink color box indicates the central TG-rich microsatellite region embedded within highly conserved regions (grey boxes). Primer sequences used for amplification are indicated with black arrows. Numbers in brackets after the strain name indicate the number of independent positive sequencings, numbers at the 3' end indicate the size of the PCR product and the number of TG-repeats (bold). Red writings indicate transcriptomic (t) or genomic (g) sequences available on the HydrATLAS (HA) server [32, 40, 41], the NHGRI *Hydra* web portal for the *Hydra* 2.0 genome (g2.0) [34] and Juliano transcriptomes (Jul) [38] or the Compagen (Co) server [37, 42] (see **S2 Table**). **(C)** Graphical representation of the different *ms-c25145* amplicons as deduced from sequencing data. Each dot corresponds to a distinct amplicon confirmed by one or several sequencings as indicated by the number of sequenced colonies (see **S2 Table**). Green, red and yellow color dots correspond to expected sizes, lighter color dots refer to sequences with errors (PCR or sequencing), the grey dot indicates missing data.

https://doi.org/10.1371/journal.pone.0230547.g004

216 bp long, and a smear of larger and less intense bands (**Fig 4A**, yellow arrows). This pattern is quite distinct from the sharp bands observed in *Basel2*. An intense band of similar size than in *AEPs* (218 bp) is observed for *Ho_CS* and *Ho_CR* as well as some weaker and longer amplicon (**Fig 4A**, orange arrows). In summary, *ms-c25145* appears as an informative marker to distinguish *Hm-105*, *Basel1* and *Basel2* strains from each other, and from strains representative of the *H. carnea*, *H. oligactis* and *H. viridissima* species.

To confirm these results, we cloned the PCR products and randomly sequenced some colonies from at least two animals of each strain (for sequencing details see **S2 Table**), and we found the sequence size fully consistent with the observed size of the bands on the gels (**Fig 4B and 4C**). Indeed, the lowest *Basel1* PCR product is slightly shorter (205 bp) than the unique *Basel2* PCR product (207 bp), whereas the two other *Basel1* PCR products are 217 and 220 bp long. For *Hm-105*, we retrieved sequences for three PCR products out of the four observed on the gel, two corresponding to the shortest bands (192 and 203 bp) and one to the upper one (223–225 bp). In *AEP* samples, we retrieved multiples sequences with nucleotide polymorphism (AA instead of CA repeat) that correspond to the most abundant PCR product, ranging from 212 to 218 pb. Finally, sequencing results confirmed that the main PCR product observed in *H. oligactis* strains correspond to the 218 bp band, also found in *AEPs*. The sequencing data provided robust results regarding the number of TG-repeats of each sequence, i.e. 6, 13 and 17 in *Hm-105*, 7 and 13 in *Basel1*, 8 in *Basel2*, and 14 in the *H. carnea* and *H. oligactis* sequences.

We also analyzed the location of this *ms-cv25145* microsatellite sequence within the *ms-cv25145* gene: It appears intronic, located after the first exon, about 245 bp downstream to the 5' end (**S2 Fig**). In all *Hydra* strains where this microsatellite was detected, we actually also retrieved at least one isoform that does not contain the intronic region indicating that the unprocessed and the mature *c25145* transcripts are rather stable. The *c25145* gene encodes a putative evolutionarily-conserved protein with an unknown function as deduced from the alignment of the *Hydra* c25145 deduced protein product with related bilaterian sequences (**S4 Fig**). We found similarities in the N-terminal moiety (~100 first amino acids) with hypothetical proteins expressed by the sea cucumber *Apostichopus japonicus* [51], the arthropods *Folsomia candida* and *Sipha flava* (aphid), the mollusc *Crassostrea gigas*, the teleost fish *Myripristis murdjan*, *Sinocyclocheilus rhinocerous* or *Danio rerio*. Within this domain, a signature can be identified, formed of 37 residues, from which 32 are present in the *Hydra* protein (**S4 Fig**).

The *ms-AIP* polymorphism helps to identify *H. vulgaris-Pallas* and *H. vulgaris*-NA strains

The second microsatellite region (*ms-AIP*) is an AT-rich region located in the 5'UTR region of the gene encoding the Aryl-hydrocarbon (AH) receptor-Interacting Protein (**S5 Fig**). The polymorphism of *ms-AIP* is more restricted than that of *ms-c25145*, as we were unable to

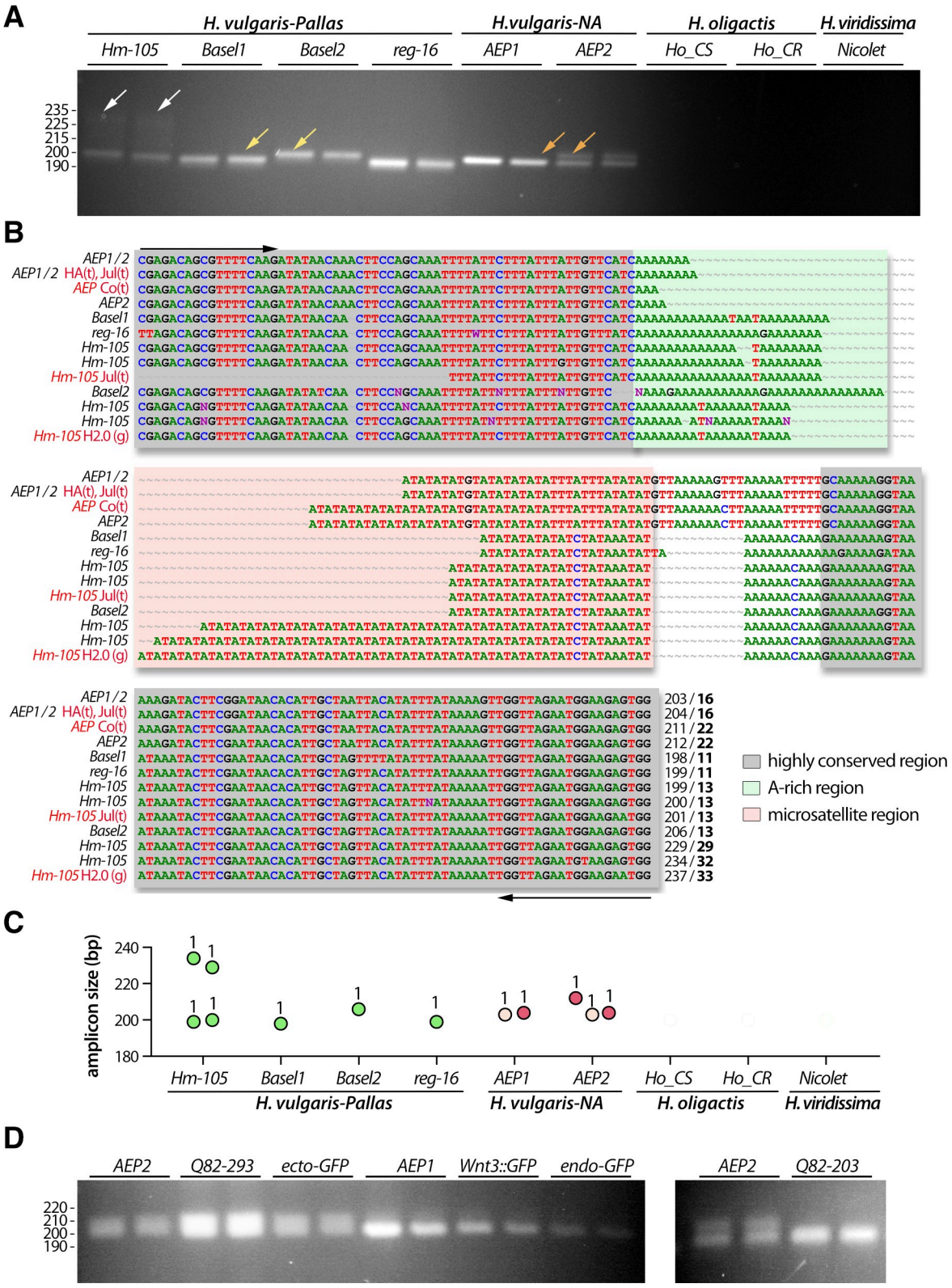

Fig 5. Analysis of the polymorphism of the AT-rich microsatellite region of the *Aryl-Hydrocarbon Receptor-Interacting Protein gene (ms-AIP).* (A) Amplification of the *ms-AIP* genomic sequences in six out of nine tested strains, which represent two distinct *H. vulgaris* sub-groups, *H. vulgaris-Pallas* (*Basel1*, *Basel2*, *Hm-105*, *reg-16*) and *H. vulgaris-NA* (*AEP1*, *AEP2*). White arrows point to a faint band

observed only in *Hm-105* polyps, yellow arrows indicate a size difference between *Basel1* and *Basel2*, and the orange arrows show a second band detected in *AEP2* but not in *AEP1*. (B) Alignment of the *ms-AIP* sequences. The color boxes indicate the AT-rich central region (salmon-pink) and an A-rich motif (green) embedded within highly conserved regions (grey). Primer sequences used for amplification are indicated with black arrows. Numbers at the 3' end indicate the PCR product size and the number of AT-repeats (bold). Red writings indicate transcriptomic (t) or genomic (g) sequences available on HydrATLAS (HA) [32, 40, 41], NHGRI web portal for the *Hydra* 2.0 genome (g2.0) [34] and Juliano transcriptomes (Jul) [38], or Compagen (Co) server [37, 42] (see S2 Table). (C) Graphical representation of the *ms-AIP* amplicons as deduced from sequencing data. Dot legend as in Fig 4. (D) Amplification of *ms-AIP* in five transgenic lines *ecto-GFP* and *endo-GFP* produced in uncharacterized AEP [42], *AEP1_Wnt3* [49], *AEP2_203* and *AEP2_293* (QS, unpublished).

https://doi.org/10.1371/journal.pone.0230547.g005

amplify these genomic sequences from the *H. oligactis* and *H. viridissima* strains (Fig 5A). Nevertheless, *ms-AIP* is useful to discriminate between the strains within the *H. vulgaris group*, i.e. *Hm-105*, *reg-16*, *Basel1*, *Basel2*, *AEP1*, *AEP2*. Two PCR products were obtained after genomic amplification from *Hm-105* and *AEP2* whereas a single PCR product was amplified from the other strains, with a specific size for each strain (Fig 5A).

The sequencing results mainly matched with the patterns detected by electrophoresis (Fig 5B and 5C), proving that distinct band sizes reflected stable strain-specific variations in both the length of the A-rich region and the number of AT-repeats. Indeed, two distinct batches of sequences were obtained for *Hm-105* (199–200 and 229–234 pb; 13 and 29–33 AT-repeats respectively). The slight differences observed in the amplicon size among a given animal possibly resulted from polymerase slippage during the PCR process or from an altered sequencing process, as often observed in AT-rich regions (Fig 5B). In addition, the *ms-AIP* sequences obtained from *Basel1*, *Basel2* and *reg-16* are consistent with the 198, 206 and 199 pb long bands observed on the gels, corresponding to 11, 13 and 11 AT-repeats respectively. In contrast to *ms-c25145*, the analysis of the *ms-AIP* sequences helps distinguish between *AEP1* and *AEP2*, since *AEP2* shows two bands, 204 and 212 bp long corresponding to 16 and 22 AT-repeats, while only the lowest band is present in *AEP1* (Fig 5A, orange arrow). As a consequence, we consider *AEP1* and *AEP2* as two distinct strains even though their *COI* and *16S* sequences are identical (Fig 2). Since we were able to identify different patterns in the *AEP1* and *AEP2* strains, we also looked at the *ms-AIP* polymorphism in *AEP* transgenic lines (Fig 5D). The *Q82-293* and *ecto-GFP* lines show the two-bands pattern found in *AEP2* while the *Wnt3*::*GFP*, *endo-GFP* and *Q82-203* lines show the same single-band pattern than *AEP1*. In summary, the analysis of the *ms-AIP* patterns are informative to identify and characterize strains of the *H. vulgaris 1* species. In addition, in contrast to *ms-c25145*, *ms-AIP* provides a useful marker for the *AEP* strains and *AEP* transgenic lines.

The *ms-DMTF1* microsatellite helps to discriminate between the AEP lines

The third microsatellite sequence (*ms-DMTF1*) is also AT-rich but located in the 3' UTR of the *cyclin-D-binding Myb-Like transcription factor 1* gene (S6 Fig). The *ms-DMTF1* primers were designed for *H. vulgaris-NA* strains and are thus only suitable for strains that belong to the *H. vulgaris* group (Fig 6A). Accordingly, they are useful to discriminate between animals of this *H. vulgaris* group. The analysis of the *ms-DMTF1* polymorphism does not show variability between *AEP1* and *AEP2* but remains useful to distinguish the *endo-GFP* transgenic animals from all other *AEPs* (Fig 6). In fact, all the AEP strains and lines we tested here but the transgenic line *endo-GFP*, provide a two-band pattern, the lowest band being similar in size with the single one found in the *endo-GFP* (Fig 6B). By shot-gun sequencing of the PCRs products from different *AEP* animals, we found that the sequence of the upper band is 118 bp long (Fig 6C and 6D). In complement, the sequencing data obtained in the *endo-GFP* animals identified a PCR product that corresponds to 104 bp. Interestingly, available transcriptomes confirm the existence of both sequences (Fig 6C and S2 Table).

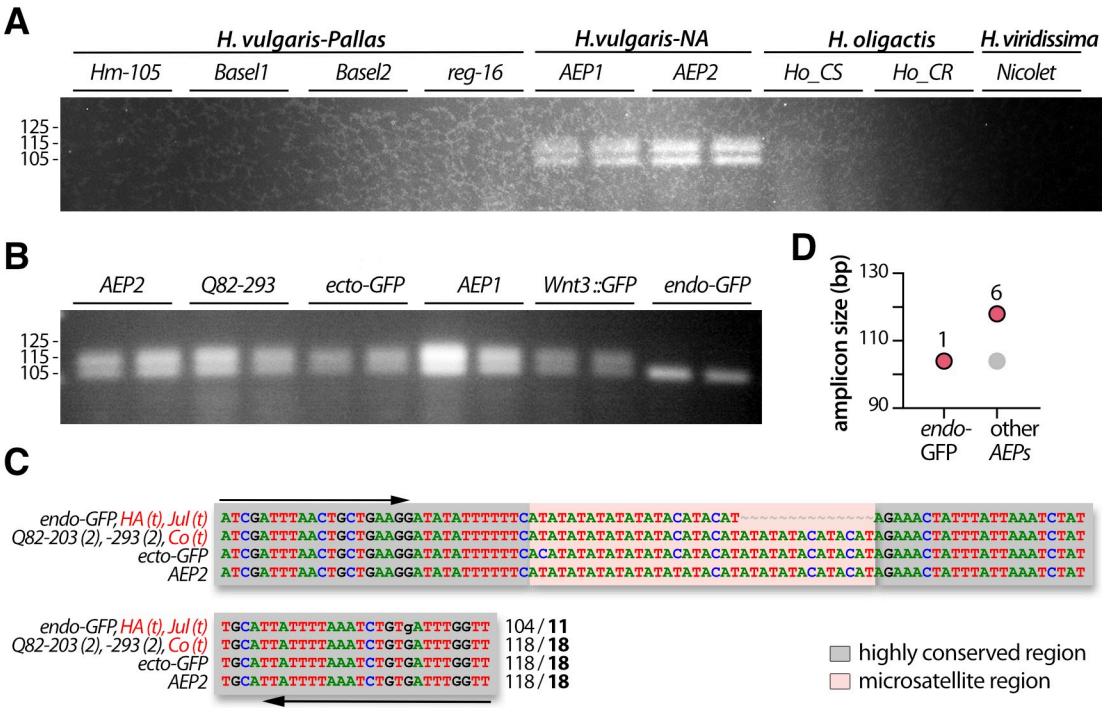

Fig 6. Analysis of the polymorphism of the AT-rich microsatellite detected in the *Cyclin-D-Binding Myb-Like Transcription Factor 1 gene (ms-DMTF1).* (A, B) Amplification of the *ms-DMTF1* genomic sequence is restricted to the *AEP* strains, either unmodified (*AEP1*, *AEP2*) or transgenic (*Q82-293*, *ecto-GFP*, *Wnt3*::*GFP*, *endo-GFP*) lines. **(C)** Alignment of the *ms-DMTF1* sequences. The color boxes indicate the AT-rich central region (salmon-pink) embedded within highly conserved regions (grey). Primer sequences used for amplification are indicated with black arrows. Numbers in brackets after the strain name indicate the number of independent positive sequencings, numbers at the 3' end indicate the size of the PCR product and the number of AT-repeats (bold). Red writings indicate transcriptomic (t) or genomic (g) sequences available on HydrATLAS (HA) server [32, 40, 41], NHGRI web portal for the *Hydra* 2.0 genome (g2.0) [34] and Juliano transcriptomes (Jul) [38], or Compagen (Co) server [37, 42] (see **S2 Table**). **(D)** Graphical representation of the size of the *ms-DMTF1* amplicons as deduced from sequencing data. Red color dots correspond to expected sizes, the grey dot indicates missing data.

https://doi.org/10.1371/journal.pone.0230547.g006

Comparative analysis of the information brought by microsatellite barcoding

To establish the respective barcode values of the *ms-c25145*, *ms-AIP* and *ms-DMTF1* microsatellites (**Fig 7**), we compared the results obtained in the 36 strain/species pairs tested for each microsatellite. From the analysis of these three microsatellites we deduced four levels of information, (1) informative when the patterns are distinct between the two strains/species, (2) partially informative when microsatellite amplification is observed in one strain/species but not in the other, (3) or when the patterns obtained are identical between the two strains/species, (4) non-informative when amplification is not observed in either strain/species.

Among these three microsatellites, *ms-c25145* is the most informative as the only one amplified in three distinct groups (*H. vulgaris-Pallas*, *H. vulgaris-NA*, *H. oligactis*), providing a positive discrimination in 29 pairs (80.6%), either based on specific patterns as observed in 15 pairs (41.7%) or on an amplification restricted to a single strain/species in 14 pairs (38.9%). The *ms-AIP* is amplified in *H. vulgaris-Pallas* and *H. vulgaris-NA*, providing a positive discrimination in 30 pairs, based on specific patterns in only 12 pairs (40%) and on an amplification restricted to a single strain/species in 18 pairs (60%). Finally, *ms-DMTF1* is only amplified in the *AEP1* and *AEP2* strains, providing a similar pattern in eight pairs, but a distinct one in some transgenic strains. We concluded that the approach presented here fulfilled our initial objective since it allowed us to properly characterize all strains of the *H. vulgaris* group used in

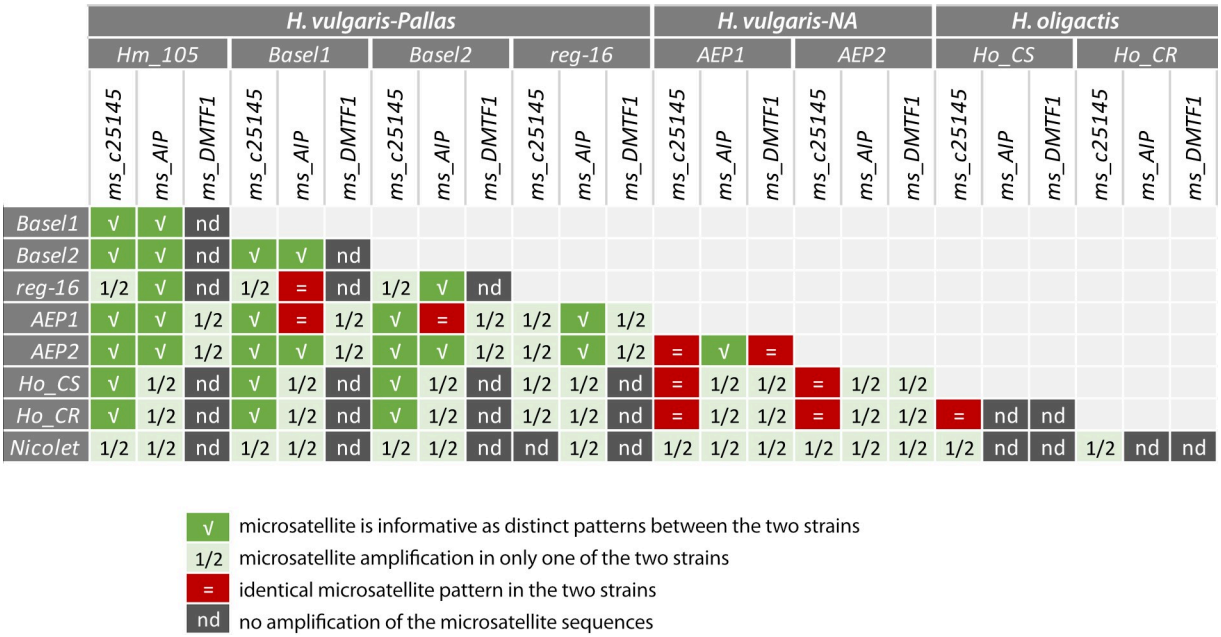

Fig 7. Summary scheme showing the value of each microsatellite for efficient discrimination between *Hydra* species and *Hydra* strains.

https://doi.org/10.1371/journal.pone.0230547.g007

our laboratory, i.e. strains *Hm-105*, *Basel1*, *Basel2* and *reg-16* of the species *H. vulgaris-Pallas* as well as strains *AEP1*, *APE2* of the species *H. vulgaris-NA*. By contrast, the phylogenetic approaches based on *COI* and *16S* sequences to discriminate between strains had failed as the *COI* and *16S* sequences were identical between some strains.

Analysis of speciation events in *H. vulgaris* based on the microsatellite signatures

Although the region surrounding the microsatellites sequences is quite conserved between all strains, we observed systematic differences between *H. vulgaris-Pallas* and *H. vulgaris-NA* strains in the organization of the amplified regions such as the TAGTCAAAGTAGTACA deletion in the upstream non-conserved region of *ms-c25145* in *H. vulgaris-Pallas* strains (**Fig 4B**), or the size difference in the A-rich region in *ms-AIP* (**Fig 5B**). The conserved deletions in one of the two subgroups and the differences in the microsatellite motifs might suggest that the genetic flux between *H. vulgaris-NA (AEP)* and *H. vulgaris 1* strains (*Hm-101*, *Basel1*, *Basel2*, *reg-16*) no longer exists. This result is compatible with the hypothesis that *H. vulgaris-Pallas* and *H. vulgaris-NA* can be considered as two cryptic species [52]. This hypothesis requires further confirmation such as the amplification of the *ms-c25145*, *ms-AIP* and additional microsatellite sequences from representative animals of the 14 hypothetical species reported by Schwentner and Bosch [16]. The acquisition of a genome for each sub-group would help to perform meta-analyses and analysis of single-nucleotide polymorphism to characterize the *H. vulgaris* species as recently done for the *Ophioderma* sea stars [53].

Discussion

The direct dissociation of soft tissues provides quality templates for genomic PCR amplification

Genomic extractions for multiple samples as well as for population genetics studies can be rapid but costly when commercial kits are used, or time-consuming and risky when reagents

that are rather toxic to humans and/or the environment are used (e.g. guanidium thiocyanate, β-mercaptoethanol). For these reasons, a procedure using a simple buffer containing proteinase K has previously been established for efficient DNA extraction from individual *Hydra* polyps [15]. Here, we have simplified this procedure to completely bypass the genomic extraction step and to use directly as PCR substrate dissociated *Hydra* tissues that we call "macerate extracts". The rapid, inexpensive and highly reproducible single-step protocol is based on the mechanical dissociation of the tissues, which reliably allows the PCR amplification of mitochondrial and nuclear DNA. This procedure is now commonly used in our laboratory, not only to amplify microsatellite sequences and detect in *Hydra* cultures suspected contamination between strains, but also to amplify genomic sequences of genes of interest for directly sequencing or insertion into plasmid vectors. We also successfully applied this procedure to PFA-fixed *Hydra* tissues as reported above, as well as poriferan larvae (e.g. *Oscarella lobularis*, not shown). Nevertheless, if this direct DNA amplification from fixed animals provides a genomic DNA from similar quality that that obtained from fresh animals, it is quantitatively less efficient. In summary, this protocol can be effectively applied to soft tissues from any developing or adult organisms, especially when small amounts of tissue are available.

Systematize characterization of *Hydra* strains to improve data reproducibility

The microsatellite barcoding approach reported here offers a series of important advantages in that it is (i) *sensitive*, detecting a 2 bp shift in amplicon size, (ii) *simple*, requiring no chemicals or materials other than those used in ordinary PCR as in conventional barcoding approaches, (iii) *fast*, with data being acquired in less than a day, (iv) *robust* as it provides reproducible results, with 100% specific PCR amplification when primer sequences are evolutionarily-conserved. The immediate use of macerate extracts could be a possible limitation of this procedure. Indeed, we did not test the quality of these macerate extracts after their storage in a frozen state, assuming that nucleic acid degradation would occur. Nevertheless, we were able to amplify genomic DNA obtained after mechanical dissociation from fixed animal samples, implying that fresh material is not an absolute requirement.

In the context of life sciences where reproducibility can be a challenge [54, 55], the development of tools to properly characterize the animals we work with appears to be a cornerstone towards more effective research. Indeed, *Hydra* laboratories use a wide variety of strains that are known to respond differently to chemical treatments or show variable sensitivity to gene expression silencing by RNAi. This procedure opens up the possibility of conducting blind clonal culture experiments, where the sensitivity of different strains to toxic substances, environmental stresses such as temperature changes can be compared. Indeed, as the microsatellite barcode procedure can be easily replicated on batches of unique polyps, it represents a major asset for discriminating among phenotypically similar polyps those that are genetically different, and vice versa. For novel unknown strains, it might be necessary to first identify additional microsatellite regions.

Possible mechanisms explaining the strain-specific variations observed in *Hydra* microsatellite sequences

Karyotyping on *Hm-105* revealed that *Hydra* are diploid animals (2n = 30) [56]. It is therefore not surprising to observe either a single band or more frequently the same band completed by a second band, reflecting the homozygous versus heterozygous status of a given animal respectively. On the other hand, we interpret the differences in band size observed in animals of different strains as different alleles. Nevertheless, we have clearly observed and sequenced more

than two different bands in the same polyp (see *ms-c25145 in Hm-105* and *Basel1*). As mentioned above, the *ms-c25145* primers we have designed can amplify two different regions of the *Hm-105* genome (*Sc4wPen_1246*, *Sc4wPen_396*), which explains why four bands can be observed in this strain (twice two alleles). The most parsimonious scenario would be that these two regions result from a recent single gene duplication that occurred in the common ancestor of the *Hm-105* and *Basel1* strains, without affecting the other strains tested here where only one copy is detected.

The microsatellite barcoding might also reveal some genetic mosaicism, as suspected from the four-band and three-band patterns observed for *ms-c25145*. Genetic mosaicism is defined as genetic variations acquired post-zygotically in cells of an individual developed from a single zygote, a phenomena frequently observed in plants and clonal animals as well as in humans [57, 58]. In clonal animals as cnidarians, the segregation of germ cells does not occur during early embryonic development and mutations affecting somatic cells as well as germ cells can accumulate over the multiple divisions of multipotent stem cells. In *Hydra*, beside the interstitial stem cell population that can transiently provide germ cells, the two epithelial stem cell populations also continuously cycle over the lifetime of the animal, potentially accumulating somatic mutations independently. This mechanism provides the opportunity for additional genetic variations within the same animal as observed in leaf cells [59].

Conclusion

With this study, we implemented a powerful barcoding approach based on microsatellite polymorphism for strains belonging to the *H. vulgaris* group. The use of this approach should enhance the reproducibility of experiments conducted in different laboratories by allowing the correct identification of each strain, including the AEP transgenic lines, in order to conduct unbiased experiments on well-characterized polyps. Data obtained on six wild-type strains belonging to the main *Hydra* species used in experimental biology, namely *H. vulgaris-Pallas* and *H. vulgaris-NA*, tend to confirm that the *H. vulgaris* group actually covers a set of cryptic species rather than a single one. We believe that microsatellite polymorphism analysis can help discover speciation events, thus representing a complementary approach to phylogenetic analyses aimed at identifying *Hydra* species.

Supporting information

S1 Table. Accession numbers of the *16S* ribosomal RNA and *Cytochrome C Oxydase I (COI)* sequences.
(DOCX)

S2 Table. Accession numbers of the *ms-c25145*, *ms-AIP*, *ms-DMTF1* microsatellite sequences.
(DOCX)

S1 Fig. Phylogenetic reconstruction of the *Hydra* genus based on the analysis of the 16S ribosomal RNA sequences.
(DOCX)

S2 Fig. Alignment of the *Hydra* genomic and transcriptomic *ms-c25145* sequences.
(DOCX)

S3 Fig. Reproducibility of the amplified patterns corresponding to the *ms-c25145* region.
(DOCX)

S4 Fig. Alignment of the putative *Hydra* c25145 protein with related gene products identified in bilaterian species.
(DOCX)

S5 Fig. Alignment of the *ms-AIP Hydra* genomic and transcriptomic sequences and expression profiles.
(DOCX)

S6 Fig. Alignment of the *Hydra* transcriptomic and genomic sequences corresponding to *ms-DMTF1*.
(DOCX)

S7 Fig. Expression profile of the *Hydra DMTF1* gene.
(DOCX)

S8 Fig. Intact gels used in the panels shown in Figs 2A, 4A, 5A, 6A and in S3 Fig.
(DOCX)

Author Contributions

Conceptualization: Quentin Schenkelaars.

Data curation: Quentin Schenkelaars, Brigitte Galliot.

Formal analysis: Quentin Schenkelaars, Brigitte Galliot.

Funding acquisition: Brigitte Galliot.

Investigation: Diego Perez-Cortes, Chrystelle Perruchoud.

Methodology: Quentin Schenkelaars, Diego Perez-Cortes, Chrystelle Perruchoud.

Project administration: Quentin Schenkelaars, Brigitte Galliot.

Supervision: Brigitte Galliot.

Writing – original draft: Quentin Schenkelaars.

Writing – review & editing: Brigitte Galliot.

References

1. Trembley A. Mémoires pour servir à l'histoire d'un genre de polypes d'eau douce, à bras en forme de cornes. Leiden; 1744.
2. Watanabe H, Hoang VT, Mattner R, Holstein TW. Immortality and the base of multicellular life: Lessons from cnidarian stem cells. *Semin Cell Dev Biol*. 2009; 20: 1114–25. https://doi.org/10.1016/j.semcdb.2009.09.008 PMID: 19761866
3. Galliot B, Quiquand M. A two-step process in the emergence of neurogenesis. *Eur J Neurosci*. 2011; 34: 847–862. https://doi.org/10.1111/j.1460-9568.2011.07829.x PMID: 21929620
4. Galliot B. Hydra, a fruitful model system for 270 years. *Int J Dev Biol*. 2012; 56: 411–423. https://doi.org/10.1387/ijdb.120086bg PMID: 22855328
5. Augustin R, Fraune S, Franzenburg S, Bosch TC. Where simplicity meets complexity: hydra, a model for host-microbe interactions. *Adv Exp Med Biol*. 2012; 710: 71–81. https://doi.org/10.1007/978-1-4419-5638-5_8 PMID: 22127887
6. Rachamim T, Sher D. What Hydra can teach us about chemical ecology how a simple, soft organism survives in a hostile aqueous environment. *Int J Dev Biol*. 2012; 56: 605–611. https://doi.org/10.1387/ijdb.113474tr PMID: 22689366
7. Murugadas A, Zeeshan M, Thamaraiselvi K, Ghaskadbi S, Akbarsha MA. Hydra as a model organism to decipher the toxic effects of copper oxide nanorod: Eco-toxicogenomics approach. *Sci Rep*. 2016; 15: 29663.

8. Schenkelaars Q, Boukerch S, Galliot B. Freshwater Cnidarian Hydra: A Long-lived Model for Aging Studies. In: Rattan SIS, editor. *Encyclopedia of Biomedical Gerontology*, Academic Press; 2020. p. 115–127.
9. Sugiyama T, Fugisawa T. Genetic analysis of developmental mechanisms in hydra. I. Sexual reproduction of Hydra magnipapillata and isolation of mutants. *Growth Dev Differ*. 1977; 19: 187–200.
10. Sugiyama T, Fujisawa T. Genetic analysis of developmental mechanisms in Hydra. VII. Statistical analyses of developmental morphological characters and cellular compositions. *Dev Growth Differ*. 1979; 21: 361–375.
11. Campbell RD. A new species of Hydra (Cnidaria: Hydrozoa) from North America with comments on species clusters within the genus. *Zool J Linn Soc*. 1987; 91: 253–263.
12. Holstein T, Emschermann P. Zytologie. In: Schwoerbel J, Zwick P, editors. *Cnidaria*: *Hydrozoa*, *Kamptozoa*. Stuttgart: Gustav Fisher Verlag; 1995. p. 5–15. (Süßwasserfauna von Mitteleuropa; vol. 1).
13. Hemmrich G, Anokhin B, Zacharias H, Bosch TC. Molecular phylogenetics in Hydra, a classical model in evolutionary developmental biology. *Mol Phylogenet Evol*. 2007; 44: 281–290. https://doi.org/10.1016/j.ympev.2006.10.031 PMID: 17174108
14. Kawaida H, Shimizu H, Fujisawa T, Tachida H, Kobayakawa Y. Molecular phylogenetic study in genus Hydra. *Gene*. 2010; 468: 30–40. https://doi.org/10.1016/j.gene.2010.08.002 PMID: 20708072
15. Martinez DE, Iniguez AR, Percell KM, Willner JB, Signorovitch J, Campbell RD. Phylogeny and biogeography of Hydra (Cnidaria: Hydridae) using mitochondrial and nuclear DNA sequences. *Mol Phylogenet Evol*. 2010; 57: 403–410. https://doi.org/10.1016/j.ympev.2010.06.016 PMID: 20601008
16. Schwentner M, Bosch TC. Revisiting the age, evolutionary history and species level diversity of the genus Hydra (Cnidaria: Hydrozoa). *Mol Phylogenet Evol*. 2015; 91: 41–55. https://doi.org/10.1016/j.ympev.2015.05.013 PMID: 26014206
17. Ito T. A new fresh-water polyp, Hydra magnipapillata, n. sp. from Japan. In: *Science Reports of the Tohoku University*. 1947. p. 6–10.
18. Martin VJ, Littlefield CL, Archer WE, Bode HR. Embryogenesis in hydra. *Biol Bull*. 1997; 192: 345–363. https://doi.org/10.2307/1542745 PMID: 9212444
19. Wittlieb J, Khalturin K, Lohmann JU, Anton-Erxleben F, Bosch TCG. Transgenic Hydra allow in vivo tracking of individual stem cells during morphogenesis. *Proc Natl Acad Sci U S A*. 2006; 103: 6208–6211. https://doi.org/10.1073/pnas.0510163103 PMID: 16556723
20. Schaller HC, Schmidt T, Flick K, Grimmelikhuijzen CPJ. Analysis of morphogenetic mutants of hydra. I. The aberrant. *Roux Arch Dev Biol*. 1977; 193–206.
21. Schaller HC, Schmidt T, Flick K, Grimmelikhuijzen CPJ. Analysis of morphogenetic mutants of hydra. II. The non-budding mutant. *Roux Arch Dev Biol*. 1977; 183: 207–214.
22. Schaller HC, Schmidt T, Flick K, Grimmelikhuijzen CPJ. Analysis of morphogenetic mutants of hydra. III. Maxi and Mini. *Roux Arch Dev Biol*. 1977; 183: 215–222.
23. Takano J, Sugiyama T. Genetic analysis of developmental mechanisms in hydra. XVI. Effect of food on budding and developmental gradients in a mutant strain L4. *J Embryol Exp Morphol*. 1985; 90: 123–138. PMID: 3834025
24. Sugiyama T, Fujisawa T. Genetic analysis of developmental mechanisms in Hydra. III. Characterization of a regeneration deficient strain. *J Embryol Exp Morph*. 1977; 42: 65–77.
25. Sugiyama T. Roles of head-activation and head-inhibition potentials in pattern formation of Hydra: Analysis of a multi-headed mutant strain. *Am Zool*. 1982; 22: 27–34.
26. Zeretzke S, Berking S. Analysis of a Hydra mutant which produces extra heads along its body axis. *Int J Dev Biol*. 1996; Suppl 1:271S.
27. Sugiyama T, Fujisawa T. Genetic analysis of developmental mechanisms in Hydra. II. Isolation and characterization of an interstitial cell-deficient strain. *J Cell Sci*. 1978; 29: 35–52. PMID: 627611
28. Marcum BA, Fujisawa T, Sugiyama T. A mutant hydra strain (sf-1) containing temperature-sensitive interstitial cells. In: Tardent P, Tardent R, editors. *Developmental and Cellular Biology of Coelenterates*. Amsterdam: Elsevier/North Holland; 1980. p. 429–434.
29. Chera S, Ghila L, Wenger Y, Galliot B. Injury-induced activation of the MAPK/CREB pathway triggers apoptosis-induced compensatory proliferation in hydra head regeneration. *Dev Growth Differ*. 2011; 53: 186–201. https://doi.org/10.1111/j.1440-169X.2011.01250.x PMID: 21338345
30. Glauber KM, Dana CE, Park SS, Colby DA, Noro Y, Fujisawa T, et al. A small molecule screen identifies a novel compound that induces a homeotic transformation in Hydra. *Development*. 2013; 140: 4788–4796. https://doi.org/10.1242/dev.094490 PMID: 24255098

31. Schenkelaars Q, Tomczyk S, Wenger Y, Ekundayo K, Girard V, Buzgariu W, et al. Hydra, a model system for deciphering the mechanisms of aging and resistance to aging. In: Conn PM, Ram JL, editors. *Conn's Handbook For Models On Human Aging*. 2nd ed. Elsevier; 2018.

32. Tomczyk S, Suknovic N, Schenkelaars Q, Wenger Y, Ekundayo K, Buzgariu W, et al. Deficient autophagy in epithelial stem cells drives aging in the freshwater cnidarian *Hydra*. *Development*. 2020; 147: dev177840. https://doi.org/10.1242/dev.177840 PMID: 31862842

33. David CN, Fujisawa T, Bosch TCG. Interstitial stem cell proliferation in hydra: Evidence for strain-specific regulatory signals. *Dev Biol*. 1991; 148: 501–507. https://doi.org/10.1016/0012-1606(91)90268-8 PMID: 1743398

34. Chapman JA, Kirkness EF, Simakov O, Hampson SE, Mitros T, Weinmaier T, et al. The dynamic genome of Hydra. *Nature*. 2010; 464: 592–596. https://doi.org/10.1038/nature08830 PMID: 20228792

35. Wenger Y, Galliot B. RNAseq versus genome-predicted transcriptomes: a large population of novel transcripts identified in an Illumina-454 Hydra transcriptome. *BMC Genomics*. 2013; 14: 204. https://doi.org/10.1186/1471-2164-14-204 PMID: 23530871

36. Wenger Y, Galliot B. Punctuated emergences of genetic and phenotypic innovations in eumetazoan, bilaterian, euteleostome, and hominidae ancestors. *Genome Biol Evol*. 2013; 5: 1949–1968. https://doi.org/10.1093/gbe/evt142 PMID: 24065732

37. Petersen HO, Hoger SK, Looso M, Lengfeld T, Kuhn A, Warnken U, et al. A Comprehensive Transcriptomic and Proteomic Analysis of Hydra Head Regeneration. *Mol Biol Evol*. 2015; 32: 1928–1947. https://doi.org/10.1093/molbev/msv079 PMID: 25841488

38. Juliano CE, Reich A, Liu N, Götzfried J, Zhong M, Uman S, et al. PIWI proteins and PIWI-interacting RNAs function in Hydra somatic stem cells. *Proc Natl Acad Sci U S A*. 2014 Jan 7; 111(1):337–42. https://doi.org/10.1073/pnas.1320965111 PMID: 24367095

39. Wenger Y, Buzgariu W, Reiter S, Galliot B. Injury-induced immune responses in Hydra. *Semin Immunol*. 2014; 26: 277–294. https://doi.org/10.1016/j.smim.2014.06.004 PMID: 25086685

40. Wenger Y, Buzgariu W, Galliot B. Loss of neurogenesis in *Hydra* leads to compensatory regulation of neurogenic and neurotransmission genes in epithelial cells. *Philos Trans R Soc Lond B Biol Sci*. 2016; 371: 20150040. https://doi.org/10.1098/rstb.2015.0040 PMID: 26598723

41. Wenger Y, Buzgariu W, Perruchoud C, Loichot G, Galliot B. Generic and context-dependent gene modulations during *Hydra* whole body regeneration. *bioRxiv*. 2019; 587147.

42. Hemmrich G, Khalturin K, Boehm AM, Puchert M, Anton-Erxleben F, Wittlieb J, et al. Molecular signatures of the three stem cell lineages in hydra and the emergence of stem cell function at the base of multicellularity. *Mol Biol Evol*. 2012; 29: 3267–3280. https://doi.org/10.1093/molbev/mss134 PMID: 22595987

43. Siebert S, Farrell JA, Cazet JF, Abeykoon Y, Primack AS, Schnitzler CE, et al. Stem cell differentiation trajectories in *Hydra* resolved at single-cell resolution. *Science*. 2019; 365: eaav9314. https://doi.org/10.1126/science.aav9314 PMID: 31346039

44. Vieira MLC, Santini L, Diniz AL, Munhoz C de F. Microsatellite markers: what they mean and why they are so useful. *Genet Mol Biol*. 2016; 39: 312–328. https://doi.org/10.1590/1678-4685-GMB-2016-0027 PMID: 27561112

45. Pena SDJ, Chakraborty R. Paternity testing in the DNA era. *Trends Genet*. 1994; 10: 204–209. https://doi.org/10.1016/0168-9525(94)90257-7 PMID: 8073534

46. Manjunath BC, Chandrashekar BR, Mahesh M, Vatchala Rani RM. DNA Profiling and forensic dentistry–A review of the recent concepts and trends. *J Forensic Leg Med*. 2011; 18: 191–197. https://doi.org/10.1016/j.jflm.2011.02.005 PMID: 21663865

47. Anton-Erxleben F, Thomas A, Wittlieb J, Fraune S, Bosch TC. Plasticity of epithelial cell shape in response to upstream signals: a whole-organism study using transgenic Hydra. *Zool*. 2009; 112: 185–94.

48. Nakamura Y, Tsiairis CD, Ozbek S, Holstein TW. Autoregulatory and repressive inputs localize Hydra Wnt3 to the head organizer. *Proc Natl Acad Sci U S A*. 2011; 108: 9137–9142. https://doi.org/10.1073/pnas.1018109108 PMID: 21576458

49. Vogg MC, Beccari L, Ollé LI, Rampon C, Vriz S, Perruchoud C, et al. An evolutionarily-conserved Wnt3/β-catenin/Sp5 feedback loop restricts head organizer activity in Hydra. *Nat Commun*. 2019; 10: 312. https://doi.org/10.1038/s41467-018-08242-2 PMID: 30659200

50. Guindon S, Dufayard JF, Lefort V, Anisimova M, Hordijk W, Gascuel O. New algorithms and methods to estimate maximum-likelihood phylogenies: assessing the performance of PhyML 3.0. *Syst Biol*. 2010; 59: 307–321. https://doi.org/10.1093/sysbio/syq010 PMID: 20525638

51. Zhang X, Sun L, Yuan J, Sun Y, Gao Y, Zhang L, et al. The sea cucumber genome provides insights into morphological evolution and visceral regeneration. Tyler-Smith C, editor. *PLOS Biol*. 2017; 15: e2003790. https://doi.org/10.1371/journal.pbio.2003790 PMID: 29023486

52. Bickford D, Lohman DJ, Sodhi NS, Ng PKL, Meier R, Winker K, et al. Cryptic species as a window on diversity and conservation. *Trends Ecol Evol*. 2007; 22: 148–155. https://doi.org/10.1016/j.tree.2006.11.004 PMID: 17129636

53. Weber AA-T, Stöhr S, Chenuil A. Species delimitation in the presence of strong incomplete lineage sorting and hybridization: Lessons from Ophioderma (Ophiuroidea: Echinodermata). *Mol Phylogenet Evol*. 2019; 131: 138–148. https://doi.org/10.1016/j.ympev.2018.11.014 PMID: 30468939

54. Baker M. A Nature survey lifts the lid on how researchers view the 'crisis' rocking science and what they think will help. *Nature*. 2015: 3.

55. Fanelli D. Opinion: Is science really facing a reproducibility crisis, and do we need it to? *Proc Natl Acad Sci U S A*. 2018; 115: 2628–2631. https://doi.org/10.1073/pnas.1708272114 PMID: 29531051

56. Anokhin BA, Kuznetsova VG. FISH-based karyotyping of Pelmatohydraoligactis (Pallas, 1766), Hydraoxycnida Schulze, 1914, and H.magnipapillata Ito, 1947 (Cnidaria, Hydrozoa). *Comp Cytogenet*. 2018; 12: 539–548. https://doi.org/10.3897/CompCytogen.v12i2.32120 PMID: 30613371

57. Gill DE, Chao L, Perkins SL, WolJ JB. Genetic Mosaicism in Plants and Clonal Animals. *Annu Rev Ecol Evol Syst*. 1995; 26: 423–444.

58. Campbell IM, Shaw CA, Stankiewicz P, Lupski JR. Somatic mosaicism: implications for disease and transmission genetics. *Trends Genet*. 2015; 31: 382–392. https://doi.org/10.1016/j.tig.2015.03.013 PMID: 25910407

59. Diwan D, Komazaki S, Suzuki M, Nemoto N, Aita T, Satake A, et al. Systematic genome sequence differences among leaf cells within individual trees. *BMC Genomics*. 2014; 15: 142. https://doi.org/10.1186/1471-2164-15-142 PMID: 24548431